PLOS ONE

RESEARCH ARTICLE

Short-time fractal analysis of biological autoluminescence

Martin Dlask[1], Jaromír Kukal[1], Michaela Poplová[2], Pavel Sovka[3], Michal Cifra[2]*

1 Czech Technical University, Faculty of Nuclear Sciences and Physical Engineering, Trojanova 12, Praha, Czechia, **2** Institute of Photonics and Electronics of the Czech Academy of Sciences, Chaberská 57, Praha 8, Czechia, **3** Department of Circuit Theory of the Faculty of Electrical Engineering at Czech Technical University in Prague, Technická 2, Praha 6, Czechia

* cifra@ufe.cz

Citation: Dlask M, Kukal J, Poplová M, Sovka P, Cifra M (2019) Short-time fractal analysis of biological autoluminescence. PLoS ONE 14(7): e0214427. https://doi.org/10.1371/journal.pone.0214427

Editor: Miguel Angel Sánchez Granero, Universidad de Almeria, SPAIN

Received: February 27, 2019

Accepted: July 9, 2019

Published: July 26, 2019

Data Availability Statement: All relevant data are within the manuscript and its Supporting Information files.

Funding: Authors were supported by the following grants: No. SGS17/196/OHK4/3T/14 of the Czech Technical University, CZ.02.1.01/0.0/0.0/16_019/0000765 "Research Center for Informatics" of the OP VVV MEYS, internal CTU grant SGS17/183/OHK3/3T/13 "Special Applications of Signal Processing." MC and MP acknowledge Czech Science Foundation project no. 18-23597S.

Abstract

Biological systems manifest continuous weak autoluminescence, which is present even in the absence of external stimuli. Since this autoluminescence arises from internal metabolic and physiological processes, several works suggested that it could carry information in the time series of the detected photon counts. However, there is little experimental work which would show any difference of this signal from random Poisson noise and some works were prone to artifacts due to lacking or improper reference signals. Here we apply rigorous statistical methods and advanced reference signals to test the hypothesis whether time series of autoluminescence from germinating mung beans display any intrinsic correlations. Utilizing the fractional Brownian bridge that employs short samples of time series in the method kernel, we suggest that the detected autoluminescence signal from mung beans is not totally random, but it seems to involve a process with a negative memory. Our results contribute to the development of the rigorous methodology of signal analysis of photonic biosignals.

Introduction

Practically all organisms perpetually generate weak light (300–700 nm wavelength range), too weak to be visible to naked human eye, in the course of their internal metabolic processes [1]. This light phenomenon differs from a rather bright bioluminescence which is dependent on specific enzymatic complexes present only in very specific species such as fireflies and selected jellyfish. What differentiates the general biological autoluminescence from ordinary bioluminescence is, apart from the weaker intensity, its ubiquity across biological species ranging from microorganisms [2–5] through tissue cultures [6–8], plants [9–13] up to animals [14] including human [15–17]. There are also various synonyma used in the literature describing this light phenomenon such as ultra-weak photon emission [18], ultra-weak bioluminescence [19], endogenous biological chemiluminescence [20], biophotons [21–23], etc.

Widely accepted underlying mechanism which generates biological autoluminescence (BAL) is related to a chemical generation of electron-excited states of biomolecules in the course of oxidative metabolism and oxidative stress [18, 24]. While the intensity and optical

Competing interests: The authors have declared that no competing interests exist.

spectrum properties of BAL as a factor of various influences have been widely investigated [3, 25–29], there is limited knowledge and consensus about statistical properties of BAL.

The object of our current study is the BAL time series from the seeds of mung beans that were measured using a sensitive photomultiplier setup. We decided to test the hypothesis if the BAL signals of mung beans contain any intrinsic correlations. To that end, we recorded and analyzed the time series of the BAL from mung beans. One of the ways to assess correlations in the signal employs chaos- and fractal-based approaches [30]. We focus here on the analysis of the fractal character of time series using fractional processes.

Fractional Brownian motion (fBm) and fractional Gaussian noise (fGn), introduced by Mandelbrot [31], have been intensively investigated over the last few decades. They are both dependent on Hurst [32, 33] exponent $H \in (0; 1)$ that influences their autocovariance structure. The fBm or fGn assumption of finite sample is advantageously used in many fields of research of time series analysis—in network traffic modelling [34, 35], financial time series [36, 37], or in biomedicine especially for detection of Alzheimer's disease [38] and cardiology [39].

When analyzing real-world data, the measured sample is usually discrete and short. The traditional methods are generally not suitable for short time series analysis. That is the reason why we need to use a precise method that can estimate the Hurst exponent without bias and can determine the confidence intervals of the estimate. The fractional character of data can be measured via fractional Brownian bridge model, which is a discrete process derived from traditional continuous fBm. A lot of time series are short due to their nature or cut by purpose or experimental limitations. Reconsidering some fBm properties that are taken in long time series analysis as granted and customizing them into a short-time, the discrete model allows estimating Hurst exponent of the discrete measured signal. This approach is advantageously used in a recently developed method of fractional Brownian bridge [40].

The article at first analyzes current open questions of statistical properties of biological autoluminescence. In the next section, we then describe the theory of fBm and the method of Hurst exponent estimation as well as other employed methods, whereas the last section contains the results of the analysis of experimental signals compared to computer-generated reference signals.

Statistical properties of biological autoluminescence (BAL)

Rationale for the need of understanding of BAL statistical properties

Multiple authors proposed that statistical properties of BAL time series might contain an information related to the state of biological system [41–43]. If the existence of such nontrivial statistical properties was rigorously confirmed, it would make a substantial impact on three major areas of this research field.

At first, the discovery of nontrivial statistical properties of BAL would have an impact on the understanding of the BAL generating mechanisms [18, 21]. So far, well-accepted generating mechanism of BAL [18, 24] implicitly considers BAL a weak endogenous biological chemiluminescence formed as a by-product of oxidative metabolism and oxidative stress. General chemiluminescence is typically considered to be random, arising from individual uncorrelated photon emitter molecules [44]. If any correlations in the signal were observed, one would start to ask questions what physical, chemical, and biological processes generate such correlations, hence casting the light on BAL generating mechanisms.

At second, nontrivial statistical properties might revive an interest into long-standing intriguing, yet unresolved question: does BAL enable optical communication between cells and organisms [45–48]? Underlying hypotheses for such biocommunication role of BAL usually expect that BAL carries information which can be processed by a receiver [46]. Such

information could be encoded in the intensity and optical spectrum of BAL [49] or in statistical properties of BAL, if they are any different from random light, as claimed by some authors [45].

At third, statistical properties would represent a completely novel fingerprint for application of BAL in biosensing in biotechnology, agriculture, food industry, and medicine beyond the intensity and optical spectra, hence greatly enhancing application potential of BAL analysis.

Approaches for analysis of BAL statistical properties

Quantum optics approach. Historically, the first common approach to analyze the statistical properties of the photon signals is based on quantum optics theorems and employs photocount statistics of detected photonic signal [50]. Using this approach, several authors suggested that BAL manifests quantum optical coherent properties [21] or even interpreted the observed photocount statistics in terms of quantum optical squeezed states [22, 51]. We have recently criticized the interpretation of experimental evidence claiming quantum optical and quantum coherence properties of BAL [23].

Fractal- and chaos-based signal analysis approach. We believe that it is more realistic to consider that BAL could manifest complex statistical or correlated behavior due to the nature of underlying chemical reactions [52] instead of a hypothetical biological coherent quantum field as proposed in the earlier approach. For the analysis of such complex statistical or correlated behavior, fractal or chaos-based methods seem to be appropriate. Therefore, more recent efforts in the analysis of BAL statistical properties were focused on the various measures quantifying the complexity and correlations in the time series such as Hurst exponent [53] and multifractal spectra [54].

Several works found correlations or deviations from purely random process with a trivial properties in the BAL signal [42, 43, 54]. However, in all those cases, either signals of different signal-to-noise ratio [42, 43, 54] or surrogate (randomly reshuffled time series) [43] were used as reference signals. Comparing BAL signals having different signal-to-noise (signal = net mean intensity of BAL, noise = mean value of detector noise) ratio may lead to results indicating different statistical properties due to a trivial fact: statistical properties of experimentally detected BAL signal are formed by a convolution of detector noise properties with a pure BAL properties. We demonstrated this issue on the example of Fano factor analysis, see figure 4 in [13].

Using surrogate signals might also lead to misleading interpretation in case the signal contains a certain trivial linear trend before random reshuffling—such reshuffling would eradicate any trend. We showed recently that detrending of the BAL signal is not sufficient to remove artifacts since the trend is present not only in the local mean but also in the local variance of the signal (see figures 1b and 4b in [53]). We suggest that the most reliable testing of the hypothesis of nontrivial correlation properties so far can be obtained using reference signals with well-defined properties. To that end, in our recent works, we used computer-generated Poisson signal time series superposed on the experimentally detected detector dark count times series as the control signals with signal-to-noise ratio same as the experimentally detected BAL signals [53]. Such a method for reference signal generation was also recently used in entropy analysis of BAL from model plant *Arabidopsis thaliana* and helped to correctly interpret findings of different entropy values at different stages of seed germination, see figure 6 in [20].

For the first time, we combine here the advanced approach of computer-generated reference signals [53] and a novel method based on fractional Brownian motion analysis [55] to test if BAL signals from mung beans manifest any correlations.

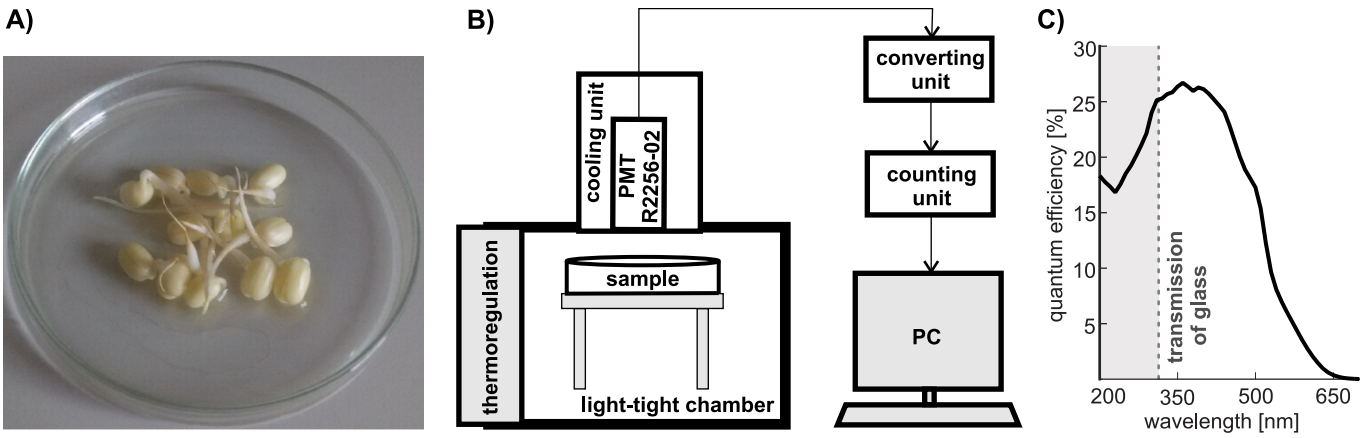

Fig 1. A: Sample of germinating mung beans. B: Scheme of the luminescence measurement setup. C: Quantum efficiency of the photomultiplier used for the detection of biological autoluminescence.

https://doi.org/10.1371/journal.pone.0214427.g001

Materials and methods

Experimental

Preparation of samples. Mung bean seeds (*Vigna radiata*, BIO Mung, CZ-BIO-001) were used as a biological material. Mung seeds were surface-sterilized with 70% ethanol for 1 min. Then, the ethanol was removed, and 50% disinfecting agent (SAVO, CZ) was added. After 10 min, the seeds were washed with distilled water 6 times and soaked for 6 h (shaken every half an hour). After the preparation, the green covers of the seeds were removed. Then, they were germinated in dark condition on large Petri dishes with ultra-pure water.

Luminescence measurement system. We used a measurement system based on cooled (-30 ˚C) low-noise photomultiplier tube (PMT) R2256-02 (all components of the system from Hamamatsu Photonics Deutschland, DE, unless noted otherwise), see Fig 1. Cooling unit C10372 (Hamamatsu Photonics Deutschland, DE) consisted of a control panel and a housing in which the PMT is placed. External water cooling is used for lower cooling temperature. High voltage power supply PS350 (Stanford Research Systems, USA) was used for powering the PMT. C9744 (converting) unit, consisting of a preamplifier, discriminator and a pulse shaping circuit, transforms photocount pulses coming from the PMT into 5V TTL pulses detected by C8855 unit connected to PC. Discriminator level was set to -500 mV and high voltage PMT supply to –1550 V based on the experimental SNR (signal-to-noise-ratio) optimization procedure performed in [56], see figure 2.13 therein.

The PMT had a dark count of ca. 17.2 s^{-1} and photocathode diameter 46 mm); see its quantum efficiency in Fig 1. PMT was mounted from the top outer side of the black light-tight chamber (standard black box, Institute of Photonics and Electronics of the Czech Academy of Sciences, Czechia). The distance between the PMT housing input window and the inner side of the bottom of the Petri dish was 3 cm.

Measurement protocol. The second day after the preparation day, 12 similar mung beans were chosen for the study and distributed into a Petri dish (5 cm in diameter), see Fig 1.

Short sequence analysis

fBm hypothesis. Fractional Brownian motion (fBm) [31] is a continuous Gaussian process $B_H(t)$ defined for continuous variable $t \in [0; +\infty)$, $H \in (0; 1)$ and $\sigma > 0$. The process starts at zero and has zero expected value for all positive times t. The autocovariance structure of

fBm obeys for all $t, s > 0$

$$\mathrm{E}(B_H(t)B_H(s)) = \frac{\sigma^2}{2}\left(|t|^{2H} + |s|^{2H} - |t-s|^{2H}\right). \quad (1)$$

Parameter H is called Hurst exponent, for $H = 1/2$, the fBm becomes Wiener process, which is standard Brownian motion. There are several cases of time series behaviour:

- $H \to 1^-$ as strongly dependent and predictable,
- $H \in (1/2; 1)$ as positive long memory process,
- $H = 1/2$ as Wiener-like process,
- $H \in (0; 1/2)$ as negative long memory process,
- $H \to 0^+$ as strongly dependent, but hardly predictable.

Discrete fractional Brownian motion of length $N \in \mathbb{N}$ is any discrete process defined for discrete variable $k = 0, \ldots, N-1$ with zero mean and autocovariance function defined for $k, l = 0, \ldots, N-1$ and $l < N-k$ as

$$\mathrm{E}(B_H(k)B_H(k+l)) = \frac{\sigma^2}{2}\left(|k|^{2H} + |k+l|^{2H} - |l|^{2H}\right). \quad (2)$$

Taking a sample of fractional Brownian motion, it is possible to investigate short samples of time series with fractional character. Finite sample $B_H(k)$ of size $N+1$ for $k = 0, \ldots, N$ of standardized fBm can be used for the construction of fractional Brownian bridge [55] in the following way

$$M_H(k) = B_H(k) - B_H(0) - \frac{k}{N}(B_H(N) - B_H(0)). \quad (3)$$

In the fractal analysis of time series, the fractional processes are often converted to fractional noises utilizing signal difference to simplify their covariance structure together with its spectral properties keeping the desired dependence on Hurst exponent. The differenced fractional Brownian bridge (dfBB) [55] is defined as

$$X_H(k) = M_H(k+1) - M_H(k) \quad (4)$$

for $k = 0, \ldots, N-1$.

Theory of dfBB. The dfBB is a discrete process and it is proven that the process has zero expected value and its variance is independent on the time lag and equals

$$\gamma_0 = 1 - N^{2H-2}. \quad (5)$$

The autocovariance of dfBB can be expressed as

$$\gamma_m = \eta(m, H) + N^{2H-2} + \frac{|m|^{2H} - |N-m|^{2H} - |N|^{2H}}{N(N-m)}, \quad (6)$$

for $m = 0, 1, \ldots N-1$ where

$$\eta(m, H) = \frac{1}{2}\left(|m+1|^{2H} - 2|m|^{2H} + |m-1|^{2H}\right) \quad (7)$$

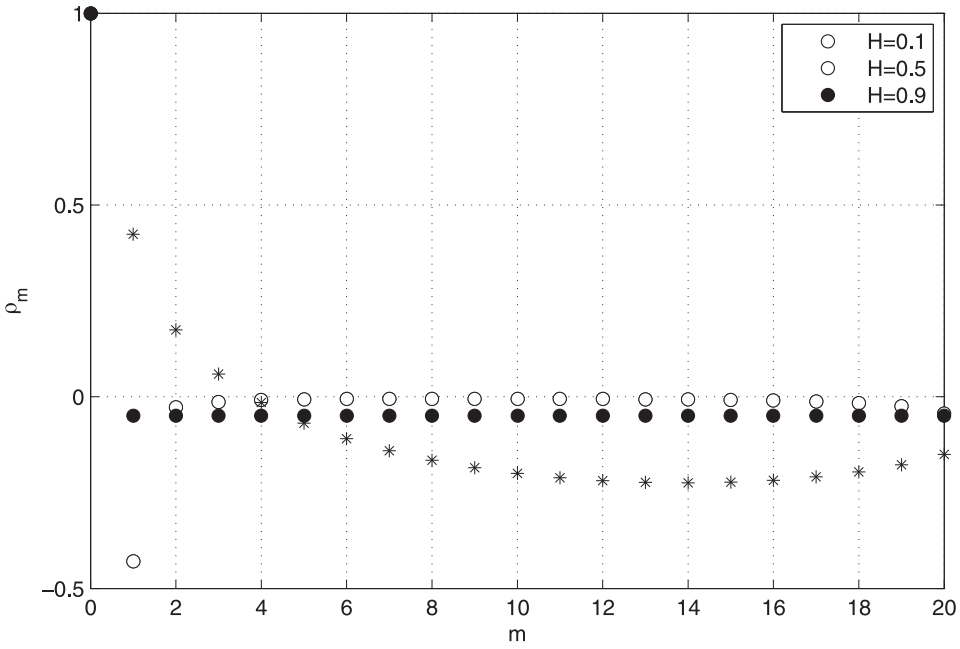

Fig 2. Autocorrelation function of dfBB for $H = 0.1$ (empty circle), $H = 0.5$ (full circle) and $H = 0.9$ (star).

https://doi.org/10.1371/journal.pone.0214427.g002

The corresponding autocorrelation function is again independent on the time lag and can be expressed as

$$\rho_m = \frac{\gamma_m}{\gamma_0} \tag{8}$$

for $m = 0, \ldots, N - 1$. The autocorrelation function of dfBB for selected H and $N = 21$ is depicted in Fig 2. This function maps non-negative integer values less than N to the autocorrelation coefficients that will be the key values for subsequent Hurst exponent estimation.

The estimation of Hurst exponent will be based on the correlation function (8). This correlation function is valid only for discrete processes that originated as sampling continuous fBm. In our work, we assume that the investigated signals have the fBm property with unknown Hurst exponent. The advantage of using dfBB is the de-trending of the input signal, which is important in the real experiment outcome analysis.

Hurst exponent estimation. The estimation of Hurst exponent is based on the fitting of the autocorrelation function. For an input discrete signal that has the fBm properties, the dfBB according to formulas (3), (4) is created. If the original signal has length $N + 1$, the respective dfBB has length N having elements $x_0, x_1, \ldots, x_{N-1}$. The estimation of n-th autocovariance coefficient $\hat{r}_n$ can be expressed for $n = 0, \ldots, N - 1$ as

$$\hat{r}_n = \frac{1}{N-n} \sum_{k=0}^{N-n-1} x_k x_{k+n} \tag{9}$$

in the case of unbiased estimation. Alternative biased estimate is based on formula

$$\hat{r}_n = \frac{1}{N} \sum_{k=0}^{N-n-1} x_k x_{k+n} \tag{10}$$

and the estimation of autocorrelation coefficient $\hat{\rho}_n$ as

$$\hat{\rho}_n = \frac{\hat{r}_n}{\hat{r}_0}. \tag{11}$$

The results using (9) and (10) were proven to be comparable, therefore we used the Eq (9) for the following calculations. Denote the theoretical value of autocorrelation from Eq (8) as $\rho_n = \rho_n(H)$ and the experimentally calculated autocorrelation as $\hat{\rho}_n$. Then we obtain the estimation of parameter H by means of solving the minimization problem

$$\hat{H} = \underset{H\in(0,1)}{\operatorname{argmin}} \sum_{j=1}^{M}\sum_{n=1}^{N-1}(\rho_{n,j} - \rho_n(H))^2, \tag{12}$$

where M is the number of signal segments. The point estimate of $\hat{H}$ was obtained by the maximum likelihood method [57] together with its standard deviation $\hat{s}$ as recommended in [55].

Likelihood ratio test

Having signal from the mung beans photon emission as well as the reference signal, we will use likelihood ratio test [58] to decide, whether the Hurst exponent of both samples is significantly different. We denote H_D as the Hurst exponent estimate of the PMT detector noise or reference signal and H_B as the Hurst exponent estimate of mung emission using the formula (12). The overall error (sum of the squares of residuals) is defined as

$$SSQ_{FULL} = \sum_{i=1}^{M}\sum_{j=1}^{N-1}(\rho^B_{i,j} - \rho_j(H_B))^2 + \sum_{i=1}^{M}\sum_{j=1}^{N-1}(\rho^D_{i,j} - \rho_j(H_D))^2, \tag{13}$$

where ρ^D, ρ^B are the autocorrelation coefficient of the noise and photon emission, respectively. The case of $j = 0$ is excluded due to $\rho^D_{i,0} = \rho_0(H_D) = 1$ for all $i = 1, .., M$. Using sub-model satisfying $H_B = H_D$ we get

$$SSQ_{SUB} = \sum_{i=1}^{M}\sum_{j=1}^{N-1}(\rho^B_{i,j} - \rho_j(H_D))^2 + \sum_{i=1}^{M}\sum_{j=1}^{N-1}(\rho^D_{i,j} - \rho_j(H_D))^2. \tag{14}$$

Using likelihood ratio (LR) test of significant difference between the sub-model and the full model, we calculate

$$\chi^2 = 2\ln\frac{L_{FULL}}{L_{SUB}} = M\cdot(N-1)\cdot\ln\frac{SSQ_{SUB}}{SSQ_{FULL}}, \tag{15}$$

where L_{FULL} and L_{SUB} are corresponding likelihoods.

When the hypothesis H_0: $H_D = H_B$ holds, i.e. the full model has the same validity as the sub-model, the criterion has χ^2_1 distribution due to single parameter constrain.

Reference signal generation. Recently we demonstrated that a suitable reference signal is crucial to understand and interpret the findings from various BAL signal analysis [20, 53]. Detector noise itself is not a suitable reference signal since it contains intrinsic technogenic correlations itself [53] and using signals of other samples with different signal-to-detector noise ratio can also lead to misleading results as we explained in section "Approaches for analysis of BAL statistical properties". Hence for this work we follow our method [53], and generated the reference signal as a sum of measured detector noise and computer-generated Poisson signal (using Matlab®2017 *poissrnd* command) with given λ in every experimental point

Table 1. Mean values of mung beans signal and noise.

T_b	200 μs	500 μs
E y_k^B	0.0115	0.0288
E y_k^D	0.0036	0.0088
λ	0.0079	0.0200

https://doi.org/10.1371/journal.pone.0214427.t001

where $\lambda = \mathrm{E}\, y_k^B - \mathrm{E}\, y_k^D$, where y_k^B and y_k^D are signal mean values of mung beans and noise, respectively. The respective values of λ in case of 200 μs signal as well as 500 μs signal are calculated in Table 1. Hence, experimentally detected BAL signals from mung beans and reference signals have practically the same mean value and same signal-to-noise ratio.

To sum up, for the analysis, we have three types of signals available:

- (B)—mung beans signal y_k^B,
- (D)—noise signal of PMT detector y_k^D,
- (R)—reference signal as a sum of measured detector noise (D) and computer-generated Poisson noise denoted as y_k^R

Results

Measurement

The investigated sample of germinating mung beans is displayed in the Fig 1. An overview of all signals collected and employed in this paper is in Table 2, where NS denotes the number of available signals.

There were two bin size settings used to collect the signals: T_s = 200 and 500 μs. For each sampling period, we have corresponding mung bean signals, detector noise signals, and computer-generated reference signals.

Both mung beans signal and PMT detector noise signal are assumed to be stationary with their mean values with the Poisson distribution. Therefore, they can be represented by their mean values E y_k^B and E y_k^D that are estimated from the measured data.

As previously mentioned, the aim of study is to compare mung beans signal with the reference signal and find statistical difference between them using their autocorrelation. With each of these two signals independently, we performed basic data processing. This procedure describes the normalization of the data, which is the essential property of fBm processes. At

Table 2. Number and type of the signals collected.

bin size T_b		200 μs	500 μs
signal type	mung beans (B)	NS = 5	NS = 5
	detector noise (D)	NS = 5	NS = 5
	reference signals (R)	NS = 5	NS = 5
number of bins in each measurement		N_b = 100 000	N_b = 100 000
length of each measurement [s]		20	50
total number of bins Q = NS × N_b		500 000	500 000
total length of all measurements per signal type [s]		100	500

https://doi.org/10.1371/journal.pone.0214427.t002

first the input time series y_k for $k = 0, 1, \ldots, Q-1$ was cumulatively summed for a window size $h \in \mathbb{N}$ and Anscombe transformation [59] was performed. The resulting signal z_k can be expressed based on the output from measuring device y_k as

$$z_k = 2 \cdot \left(\frac{3}{8} + \sum_{i=kh}^{(k+1)h-1} y_i \right)^{1/2} \tag{16}$$

for $k = 0, \ldots, M-1$. This transformations assures stationarity by terms of variance and guarantees Gaussian distribution of the resulting signal.

Hurst exponent estimates

There is no prior knowledge of optimal model length, accumulation compression, and Hurst exponent. Therefore, we will apply the maximum likelihood method of Hurst exponent estimation for the various model and segment lengths, and then we will individually test the differences in the Hurst exponent. However, there is a finite number of reasonable pairs (model length N, segment length h), which will cause the phenomenon of the multiple hypothesis testing. After the False Discovery Rate (FDR) correction, we will localize the model and segment lengths, which cause significant differences in the Hurst exponent. These pairs (h, N) will be declared as significantly sensitive to the signal differences in the Hurst exponent.

Having signals with two different bin sizes, we will use the signal bin size $T_b = 200$ μs as a training set and the signal with $T_b = 500$ μs as a verification set. Normalized mung beans and reference signals with bin size $T_b = 200$ μs and length $Q = 500\,000$ were the subject of the initial analysis. The signal accumulation of size h was applied to the signals, therefore the number of bins was $\lfloor Q/h \rfloor$. After the accumulation, the signal is divided into segments of length N. Due to the memory of fBm process, we will use only the odd segments for the calculation of autocorrelation function and the even segments are excluded. The new signal has length $\lceil \lfloor \lfloor Q/h \rfloor / N \rfloor / 2 \rceil$. Using Eq (12) and maximum likelihood method, we obtain the corresponding H_D and H_B estimates for the Hurst exponent of referential signal and mung beans, respectively. Based on these estimates, we can derive the p-values of LR test using (15) statistics.

In our case, we performed altogether $11 \times 11 = 121$ tests for $h = 1500, 1550, \ldots, 2000$ and $N = 20, 21, \ldots, 30$. Accumulation h could not be higher than 2000 due to the rapid decrease of the number of processed segments. The values $h < 1500$ caused lower event frequencies and the conversion from Poisson noise to Gaussian noise is not guaranteed. Similar reasons are for the range of parameter N. In fact, the fractional model is less discriminative for $N < 20$ and the case $N > 30$ reduces the number of segments. Due to multiple testing and obeying the Hochberg-Benjamini principle, we diminish the significance level from 0.05 to $\alpha_{FDR} = 0.000050$. The p-values as decadic logarithms are shown in Table 3.

In these settings, there were two cases where the Hurst exponent was significantly different. The results from these two cases are displayed in Table 4. The 95% interval of Hurst exponent estimates of mungo beans signal (H_B) was [0.2108, 0.5086], while the 95% interval for reference signal (H_R) was [0.4041,0.5931].

The lowest p-value was obtained in the case of $(h, N) = (1750, 24)$, which represents the segmentation into bins with duration 1750×200 μs = 350 000 μs = 0.35 sec.

As the verification set, the signal with $T_s = 500$ μs was taken into account, following the same procedure as the previous one. The accumulation parameter h was accordingly diminished to 2/5 of its previous value to guarantee the same segment length.

Table 3. Difference between the estimated Hurst exponent of mung beans (B) and reference signal (R) as ($-\log_{10} p$)-values of likelihood ratio test (15).

$h \backslash N$	20	21	22	23	24	25	26	27	28	29	30
1500	1.188	2.934	1.835	1.888	3.175	1.645	2.284	0.863	0.506	0.192	0.762
1550	1.172	1.617	0.394	0.887	1.420	1.470	0.912	2.113	1.651	0.026	0.691
1600	1.978	1.576	0.646	0.523	1.217	0.394	1.597	0.786	1.487	0.880	1.859
1650	0.990	1.616	1.127	2.024	1.209	0.651	1.635	0.909	1.906	3.573	2.927
1700	0.772	0.621	1.288	1.196	1.239	0.488	0.407	1.175	2.658	0.463	0.776
1750	1.475	2.325	1.269	3.131	**4.638**	1.535	2.370	1.017	0.726	0.412	1.945
1800	0.465	1.455	1.394	1.098	1.313	0.180	2.661	2.064	2.449	1.917	2.001
1850	2.377	2.010	1.308	0.567	1.533	2.382	3.184	**4.301**	3.328	2.418	1.968
1900	2.599	0.879	0.850	0.629	1.053	1.264	0.950	0.943	1.397	2.093	0.142
1950	2.574	0.095	0.706	1.900	2.843	2.874	3.261	2.514	3.462	2.501	2.405
2000	2.212	1.611	1.315	0.935	1.040	1.232	0.922	0.282	0.366	1.159	0.963

https://doi.org/10.1371/journal.pone.0214427.t003

Table 4. Estimated Hurst exponent values for mung beans (B) signal and reference signal (R).

h	N	H_B	H_R	p-val	$-\log_{10} p$-val
1750	24	0.4142	0.5299	2.3135×10^{-5}	4.638
1850	27	0.3569	0.4291	4.9977×10^{-5}	4.301

https://doi.org/10.1371/journal.pone.0214427.t004

We perform the verification for the combination of signals (B) and (R) similarly as in the previous case and additionally for the combination of (B) and (D). The first set of signals ((B) and (R)) will be used to test if the photon emission is not random and has a negative memory, while the results from the second set ((B) and (D)) of signals will be used to test if there is a significant difference between the cases, when the PMT detects BAL signals from mung beans compared to PMT noise. We use the significant cases from Table 4 to estimate their Hurst exponent and the results on verification set is displayed in Table 5. The variables s_1, s_2 denote the pair of signals, whereas the H_X denotes the estimation of Hurst exponent of the signal s_2.

We performed four tests, and according to Hochberg-Benjamini false discovery rate, we diminish the $\alpha_{FDR} = 0.0169$. Therefore, all four cases are considered significant, and we reject the hypothesis that the Hurst exponent of mung beans would be the same as H_X.

For comparison, we also performed a similar analysis with noise signal (D) and mungo beans signal (B) and captured the results in the Table 6. Using Hochberg-Benjamini principle, there is only one combination (h,N) = (1850,27) that is significant.

To demonstrate the efficiency of proposed method for short time series, we applied the method of power spectral analysis (PSD) [60, 61] for Hurst exponent estimation. The power spectrum $P(f)$ holds following relationship for any frequency f

$$P(f) \propto f^{-1-2H}, \tag{17}$$

Table 5. Estimated Hurst exponent values from verification dataset. $h = 700$ for 500 μs signals corresponds to $h = 1750$ for 200 μs signals.

s_1	s_2	h	N	H_B	H_X	p-val
B	R	700	24	0.4032	0.4415	0.0130
B	R	740	27	0.3761	0.4112	0.0042
B	D	700	24	0.4032	0.4378	0.0169
B	D	740	27	0.3761	0.4480	0.0054

https://doi.org/10.1371/journal.pone.0214427.t005

Table 6. Difference between the estimated Hurst exponent of mung beans (B) and noise signal (D) as ($-\log_{10} p$)-values of likelihood ratio test (15).

$h \backslash N$	20	21	22	23	24	25	26	27	28	29	30
1500	2.181	2.881	1.395	1.656	3.192	2.058	2.203	0.087	0.444	1.131	3.319
1550	2.191	1.125	0.446	0.736	0.348	2.101	0.283	2.378	1.936	1.560	0.407
1600	2.008	2.039	1.259	0.006	1.071	1.098	1.604	2.003	0.665	1.468	1.415
1650	1.230	1.535	1.334	2.804	1.249	0.914	0.858	1.470	2.923	2.190	3.056
1700	1.015	1.359	0.376	0.460	0.473	0.665	0.182	0.906	1.812	1.532	0.107
1750	0.769	1.218	0.926	0.346	1.771	2.386	0.687	0.331	1.286	1.136	1.605
1800	0.696	1.791	0.871	0.666	2.058	2.153	2.053	1.145	2.400	0.692	0.881
1850	2.891	1.967	1.349	0.297	1.051	2.343	2.754	**4.602**	3.472	0.779	1.432
1900	2.795	0.434	0.708	1.273	0.619	0.631	1.797	1.101	0.395	1.371	1.069
1950	1.657	1.694	0.386	2.885	2.373	2.199	2.504	2.292	1.651	0.926	2.209
2000	1.281	0.048	0.215	1.050	0.140	1.031	0.234	1.303	1.186	0.239	0.939

https://doi.org/10.1371/journal.pone.0214427.t006

therefore the Hurst exponent can be estimated using the maximum likelihood method in log-log chart. The results from the spectral method from training data are captured in Table 7, together with the Hurst exponent estimates of referential and mungo beans signals. The method exhibited similar results, showing that the estimates of H_B are lower than H_D; however, due to the very short signal length, the method provided huge standard deviation of the estimate. For this reason, the p-values are not significant, and all of them are above the value of 0.5. The obtained results were similar in the case of verification data as well, showing no significant records in the whole range of parameter h.

To assure the both PSD and differenced fractional Brownian bridge (DFBB) methods are unbiased, we generated artificial signal sample of length 300 using circular embedding method [62], which is an exact method for fractional Brownian motion generation. The results of this testing are captured in Table 8. While H denotes the Hurst exponent of artificially generated

Table 7. Spectral analysis of mung beans and reference signal as p-values.

h	H_B	H_R	p-val
1500	0.4366	0.4425	0.9039
1550	0.4871	0.5269	0.8210
1600	0.4661	0.4592	0.9436
1650	0.4107	0.4358	0.9202
1700	0.4551	0.4502	0.9642
1750	0.4322	0.5591	0.5625
1800	0.3827	0.4173	0.6539
1850	0.4366	0.4406	0.9043
1900	0.4257	0.4312	0.8789
1950	0.3973	0.4046	0.8462
2000	0.4715	0.6516	0.6821

https://doi.org/10.1371/journal.pone.0214427.t007

Table 8. Unbiasedness of PSD and DFBB methods as p-value.

H	H^{PSD}	s^{PSD}	p-value	H^{DFBB}	s^{DFBB}	p-value
0.35	0.4268	0.1956	0.3471	0.3513	0.0193	0.4728
0.40	0.4152	0.2211	0.4725	0.4123	0.0205	0.2741
0.45	0.4803	0.1676	0.4786	0.4335	0.0249	0.7443
0.50	0.5454	0.2198	0.4840	0.5030	0.0276	0.4566

https://doi.org/10.1371/journal.pone.0214427.t008

signal, the H^{PSD}, H^{DFBB} denote the Hurst exponent estimates and s^{PSD}, s^{DFBB} denote the standard deviation of this estimate using the PSD and DFBB method, while the p-value denotes the result of the t-test against the null hypothesis that the estimated value equals the theoretical one. Having all p-values above 0.05 significance level, we conclude that both PSD and DFBB method provide unbiased estimates.

Discussion

Results from rigorous statistical analysis and testing in Tables 3, 4, and 5 suggest that the mung beans signal has a negative memory (negative correlations, antipersistent behavior [63]) and its Hurst exponent is lower than the referential signal. How could such behavior originate in biological systems? It was proposed that the restriction of Brownian motion due to the structuring of nano- to microscale intracellular environment leads to anomalous sub-diffusion [64] characterized by Hurst exponent < 0.5 [63]. This is understandable since a cytoplasm environment displays fractal spatial structuring [65]. Since biochemical reactions (encounters of reactants) leading to BAL are taking place within the cell cytoplasm, organelles and lipid membranes [24] where anomalous sub-diffusion was observed [64, 66], it is not a great logical leap to speculate that BAL from mung bean samples could also display sub-diffusive features. Actually, it is already acknowledged that chemical reactions spatially constrained on the microscopic level may lead to fractal reaction kinetics [67–69] also in case of intracellular biochemical kinetics [70]. The 0.35 s as the time scale where we found statistically significant differences of mung bean signal Hurst exponent from that of the reference signal (Table 3) could correspond to a rate of underlying rate-limiting step of chemical reactions or processes which give rise to BAL. However, one has to be careful in the interpretation since there are many pitfalls in an accurate estimation of the Hurst exponent value from experiments [71, 72]. Although unlikely, given the nature of our experiments we can not fully exclude that the correlations we observe in mung signals are introduced by the photodetector (PMT) due to the nature of photocounting process [73, 74]. Introduction of anti-/correlations could be at the physical level of the PMT tube (after-pulsing, a temporary drop of the voltage at dynodes after ejecting electrons, . . .) or the follow-up circuitry (amplifiers). Anti-correlations of the detected counts depending on the count rate have been actually observed due to a PMT construction [74, Fig.9]. However, marked anti-correlations were present only for very high count rates ($>$ kHz) and very low quantum efficiency, which is not the case in our experiments. We also believe that the dead-time of a PMT [75] is not affecting the value of correlations we observe since the PMT dead-time is on the time scale of few hundreds of nanoseconds—several orders of magnitude smaller than the time scale of correlations we observed (0.35 s) and three orders of magnitude smaller than our bin size (200 and 500 μs).

Throughout the analysis, the lower limit for accumulation parameter h was chosen as 1500 to assure the normality of the processed data due to the sparsity of the input signal. Higher accumulation than 2000 is not useful since then we would lose the precision of estimate due to the short length of investigated time series. The minimal length of signal segment N was chosen to assure consistency of the used model, segment lengths of $N > 30$ do not significantly contribute to the higher precision of estimate [40].

Conclusion

In this work, we focused on statistical properties of biological autoluminescence from germinating mung bean sample. Our emphasis was on the development of a rigorous mathematical

and statistical methodology, which takes into account proper reference signals, likelihood ratio test, and multiple hypothesis testing effects.

We used a highly sensitive photomultiplier-based detection system to record a time series of photon counts of the mung bean sample emission and noise of the detector. Using the normalization of the input signal, we were able to employ the fractional models that allowed us to estimate Hurst exponent. Dividing the input signals into the training set and evaluating the differences in the Hurst exponent of both signals, the procedure allowed us to test our initial hypothesis on the verification signal. The resulting Hurst exponent mean value of mung bean sample time series is below the level of 1/2 which confirmed our initial hypothesis, that the biological autoluminescence displays correlations. We also proposed that this value could be related to anomalous sub-diffusive features of biochemical reactions underlying processes within mung beans, which give rise to photon emission time series. Further extensive work beyond the scope of this methodical paper needs to be carried out to test the biological ubiquity of anti-/correlations in biological autoluminescence signals and the role of the detector in the observed Hurst exponent values. Especially interesting would be an analysis of BAL statistical properties across samples with rising complexity starting from simple chemical solutions of small biomolecules through isolated cellular structures and cell suspensions up to whole tissues and organisms. Nevertheless, we believe that rigorous methodology we presented here will help to support the future research of BAL statistical properties towards a deeper understanding of BAL mechanisms as well as applications for label-free and non-invasive analysis in medicine and biotechnology using completely new signal fingerprint types.

Supporting information

S1 Data. All raw data files used in our analysis.
(ZIP)

Author Contributions

Conceptualization: Michal Cifra.

Data curation: Martin Dlask, Michal Cifra.

Formal analysis: Martin Dlask.

Funding acquisition: Michal Cifra.

Investigation: Martin Dlask, Michaela Poplová.

Methodology: Jaromír Kukal, Pavel Sovka, Michal Cifra.

Project administration: Jaromír Kukal, Michal Cifra.

Resources: Jaromír Kukal, Michal Cifra.

Software: Martin Dlask, Michaela Poplová.

Supervision: Jaromír Kukal, Pavel Sovka, Michal Cifra.

Validation: Michal Cifra.

Visualization: Martin Dlask, Michaela Poplová.

Writing – original draft: Martin Dlask, Michal Cifra.

Writing – review & editing: Jaromír Kukal, Pavel Sovka, Michal Cifra.

References

1. Kucera O, Cervinkova K, Nerudova M, Cifra M. Spectral perspective on the electromagnetic activity of cells. Current topics in medicinal chemistry. 2015; 15(6):513–522. https://doi.org/10.2174/1568026615666150225103105 PMID: 25714382
2. Tilbury R, Quickenden T. Luminescence from the yeast Candida utilis and comparisons across three genera. Luminescence. 1992; 7(4):245–253.
3. Quickenden TI, Tilbury RN. Luminescence spectra of exponential and stationary phase cultures of respiratory deficient Saccharomyces cerevisiae. Journal of Photochemistry and Photobiology B: Biology. 1991; 8(2):169–174. https://doi.org/10.1016/1011-1344(91)80055-M
4. Vogel R, Guo X, Süssmuth R. Chemiluminescence patterns from bacterial cultures undergoing bacteriophage induced mass lysis. Bioelectrochemistry and Bioenergetics. 1998; 46(1):59–64.
5. Vogel R, Süssmuth R. Weak light emission patterns from lactic acid bacteria. Luminescence. 1999; 14 (2):99–105. https://doi.org/10.1002/(SICI)1522-7243(199903/04)14:2<99::AID-BIO519>3.0.CO;2-7 PMID: 10398567
6. Burgos RCR, Červinková K, van der Laan T, Ramautar R, van Wijk EPA, Cifra M, et al. Tracking biochemical changes correlated with ultra-weak photon emission using metabolomics. Journal of Photochemistry and Photobiology B: Biology. 2016; 163:237–245. https://doi.org/10.1016/j.jphotobiol.2016.08.030
7. Burgos RCR, Schoeman JC, Winden LJv, Červinková K, Ramautar R, Van Wijk EPA, et al. Ultra-weak photon emission as a dynamic tool for monitoring oxidative stress metabolism. Scientific Reports. 2017; 7(1):1229. https://doi.org/10.1038/s41598-017-01229-x PMID: 28450732
8. Rác M, Sedlářová M, Pospíšil P. The formation of electronically excited species in the human multiple myeloma cell suspension. Scientific Reports. 2015; 5:8882. https://doi.org/10.1038/srep08882 PMID: 25744165
9. de Mello Gallep C. Ultraweak, spontaneous photon emission in seedlings: toxicological and chronobiological applications: UPE in seedlings—applications. Luminescence. 2014; 29(8):963–968. https://doi.org/10.1002/bio.2658 PMID: 24687546
10. Gallep CM, Moraes TA, Dos Santos SR, Barlow PW. Coincidence of biophoton emission by wheat seedlings during simultaneous, transcontinental germination tests. Protoplasma. 2013; 250(3):793–796. https://doi.org/10.1007/s00709-012-0447-x PMID: 23011402
11. Gallep CM, Moraes TA, Červinková K, Cifra M, Katsumata M, Barlow PW. Lunisolar tidal synchronism with biophoton emission during intercontinental wheat-seedling germination tests. Plant Signaling & Behavior. 2014; 9(5):e28671. https://doi.org/10.4161/psb.28671
12. Guo J, Zhu G, Li L, Liu H, Liang S. Ultraweak photon emission in strawberry fruit during ripening and aging is related to energy level. Open Life Sciences. 2017; 12(1). https://doi.org/10.1515/biol-2017-0046
13. Rafieiolhosseini N, Poplová M, Sasanpour P, Rafii-Tabar H, Alhossaini MR, Cifra M. Photocount statistics of ultra-weak photon emission from germinating mung bean. Journal of Photochemistry and Photobiology B: Biology. 2016; 162:50–55. https://doi.org/10.1016/j.jphotobiol.2016.06.001
14. van Wijk E, Kobayashi M, van Wijk R, van der Greef J. Imaging of Ultra-Weak Photon Emission in a Rheumatoid Arthritis Mouse Model. PLoS ONE. 2013; 8(12):e84579. https://doi.org/10.1371/journal.pone.0084579 PMID: 24386396
15. Ou-Yang H. The application of ultra-weak photon emission in dermatology. Journal of Photochemistry and Photobiology B: Biology. 2014; 139:63–70. https://doi.org/10.1016/j.jphotobiol.2013.10.003
16. Zhao X, Wijk Ev, Yan Y, Wijk Rv, Yang H, Zhang Y, et al. Ultra-weak photon emission of hands in aging prediction. Journal of Photochemistry and Photobiology B: Biology. 2016; 162:529–534. https://doi.org/10.1016/j.jphotobiol.2016.07.030
17. Zhao X, Pang J, Fu J, Wang Y, Yang M, Liu Y, et al. Spontaneous photon emission: A promising non-invasive diagnostic tool for breast cancer. Journal of Photochemistry and Photobiology B: Biology. 2017; 166:232–238. https://doi.org/10.1016/j.jphotobiol.2016.12.009
18. Cifra M, Pospíšil P. Ultra-weak photon emission from biological samples: Definition, mechanisms, properties, detection and applications. Journal of Photochemistry and Photobiology B: Biology. 2014; 139:2–10. https://doi.org/10.1016/j.jphotobiol.2014.02.009
19. Wang J, Yu Y. Relationship between ultra-weak bioluminescence and vigour or irradiation dose of irradiated wheat. Luminescence. 2009; 24(4):209–212. https://doi.org/10.1002/bio.1096 PMID: 19291806
20. Saeidfirozeh H, Shafiekhani A, Cifra M, Masoudi AA. Endogenous Chemiluminescence from Germinating Arabidopsis Thaliana Seeds. Scientific Reports. 2018; 8(1):16231. https://doi.org/10.1038/s41598-018-34485-6 PMID: 30385859

21. Popp FA, Nagl W, Li K, Scholz W, Weingärtner O, Wolf R. Biophoton emission: New evidence for coherence and DNA as source. Cell Biochemistry and Biophysics. 1984; 6(1):33–52. https://doi.org/10.1007/BF02788579

22. Bajpai RP. Biophoton emission in a squeezed state from a sample of Parmelia tinctorum. Physics Letters A. 2004; 322(1-2):131–136. https://doi.org/10.1016/j.physleta.2003.12.050

23. Cifra M, Brouder C, Nerudová M, Kučera O. Biophotons, coherence and photocount statistics: A critical review. Journal of Luminescence. 2015; 164:38–51. https://doi.org/10.1016/j.jlumin.2015.03.020

24. Pospíšil P, Prasad A, Rác M. Role of reactive oxygen species in ultra-weak photon emission in biological systems. Journal of Photochemistry and Photobiology B: Biology. 2014; 139:11–23. https://doi.org/10.1016/j.jphotobiol.2014.02.008

25. Prasad A, Pospísil P. Ultraweak photon emission induced by visible light and ultraviolet A radiation via photoactivated skin chromophores: in vivo charge coupled device imaging. Journal of biomedical optics. 2012; 17(8):085004. https://doi.org/10.1117/1.JBO.17.8.085004 PMID: 23224187

26. Yang M, Pang J, Liu J, Liu Y, Fan H, Han J. Spectral discrimination between healthy people and cold patients using spontaneous photon emission. Biomedical Optics Express. 2015; 6(4):1331. https://doi.org/10.1364/BOE.6.001331 PMID: 25909016

27. Kobayashi M, Iwasa T, Tada M. Polychromatic spectral pattern analysis of ultra-weak photon emissions from a human body. Journal of Photochemistry and Photobiology B: Biology. 2016; 159:186–190. https://doi.org/10.1016/j.jphotobiol.2016.03.037

28. Nerudová M, Červinková K, Hašek J, Cifra M. Optical spectral analysis of ultra-weak photon emission from tissue culture and yeast cells. In: Tománek P, Senderáková D, Páta P, editors. SPIE Proceedings; 2015. p. 94500O. Available from: http://proceedings.spiedigitallibrary.org/proceeding.aspx?doi=10.1117/12.2069897.

29. Zhao X, Yang M, Wang Y, Pang J, Wijk EV, Liu Y, et al. Spectrum of spontaneous photon emission as a promising biophysical indicator for breast cancer research. Scientific Reports. 2017; 7(1).

30. Eke A, Herman P, Kocsis L, Kozak LR. Fractal characterization of complexity in temporal physiological signals. Physiological Measurement. 2002; 23(1):R1–R38. https://doi.org/10.1088/0967-3334/23/1/201 PMID: 11876246

31. Mandelbrot B, Ness JV. Fractional Brownian Motions, Fractional Noises and Applications. SIAM Review. 1968; 10(4):422–437. https://doi.org/10.1137/1010093

32. Hurst HE. Methods of Using Long-Term Storage in Reservoirs. Proceedings of the Institution of Civil Engineers. 1956; 5(5):519–543. https://doi.org/10.1680/iicep.1956.11503

33. Julian M, Alcaraz R, Rieta JJ. Application of Hurst exponents to assess atrial reverse remodeling in paroxysmal atrial fibrillation. Physiol Meas. 2015; 36(11):2231–2246. https://doi.org/10.1088/0967-3334/36/11/2231 PMID: 26393825

34. Erramilli A, Willinger W, Pruthi P. Fractal traffic flows in high-speed communications networks. Fractals. 1994; 2(03):409–412. https://doi.org/10.1142/S0218348X94000545

35. Li D, Fan Q. Multi-fractal Modeling of Network Video Traffic and Performance Analysis. Journal of Internet Technology. 2018; 19(7):2089–2095.

36. Dubovikov MM, Starchenko NV, Dubovikov MS. Dimension of the minimal cover and fractal analysis of time series. Physica A: Statistical Mechanics and its Applications. 2004; 339(3-4):591–608. https://doi.org/10.1016/j.physa.2004.03.025

37. Bohdalová M, Greguš M. Fractal Analysis of Forward Exchange Rates. Acta Polytechnica Hungarica. 2010; 7(4):14.

38. Dlask M, Kukal J, Sovka P. Fractional Brownian Bridge Model for Alzheimer Disease Detection from EEG Signal. In: 2018 International Conference on Signal Processing and Information Security (ICSPIS); 2018. p. 1–4.

39. Captur G, Karperien AL, Hughes AD, Francis DP, Moon JC. The fractal heart—embracing mathematics in the cardiology clinic. Nature Reviews Cardiology. 2017; 14(1):56–64. https://doi.org/10.1038/nrcardio.2016.161 PMID: 27708281

40. Dlask M, Kukal J. Hurst exponent estimation from short time series. Signal, Image and Video Processing. 2018;.

41. Kobayashi M, Inaba H. Photon statistics and correlation analysis of ultraweak light originating from living organisms for extraction of biological information. Applied Optics. 2000; 39(1):183–192. https://doi.org/10.1364/ao.39.000183 PMID: 18337887

42. Van Wijk R, Van Wijk EPA, Bajpai RP. Photocount distribution of photons emitted from three sites of a human body. Journal of Photochemistry and Photobiology B: Biology. 2006; 84(1):46–55. https://doi.org/10.1016/j.jphotobiol.2006.01.010

43. Van Wijk EPA, Wijk RV, Bajpai RP, van der Greef J. Statistical analysis of the spontaneously emitted photon signals from palm and dorsal sides of both hands in human subjects. Journal of Photochemistry and Photobiology B: Biology. 2010; 99(3):133–143. https://doi.org/10.1016/j.jphotobiol.2010.03.008

44. Collinson MM, Wightman RM. Observation of individual chemical reactions in solution. Science. 1995; 268(5219):1883. https://doi.org/10.1126/science.268.5219.1883 PMID: 17797530

45. Budagovsky AV. On the ability of cells to distinguish the coherence of optical radiation. Quantum Electronics. 2005; 35(4):369–374. https://doi.org/10.1070/QE2005v035n04ABEH002837

46. Kučera O, Cifra M. Cell-to-cell signaling through light: just a ghost of chance? Cell Communication and Signaling. 2013; 11(1):1.

47. Prasad A, Rossi C, Lamponi S, Pospíšil P, Foletti A. New perspective in cell communication: Potential role of ultra-weak photon emission. Journal of Photochemistry and Photobiology B: Biology. 2014; 139:47–53. https://doi.org/10.1016/j.jphotobiol.2014.03.004

48. Scholkmann F, Fels D, Cifra M. Non-chemical and non-contact cell-to-cell communication: a short review. American journal of translational research. 2013; 5(6):586. PMID: 24093056

49. Laager F. Light based cellular interactions: hypotheses and perspectives. Frontiers in Physics. 2015; 3. https://doi.org/10.3389/fphy.2015.00055

50. Walls DF, Milburn GJ. Quantum optics. Springer; 2008.

51. Bajpai RP. Squeezed state description of spectral decompositions of a biophoton signal. Physics Letters A. 2005; 337(4-6):265–273. https://doi.org/10.1016/j.physleta.2005.01.079

52. Iranifam M, Segundo MA, Santos JLM, Lima JLFC, Sorouraddin MH. Oscillating chemiluminescence systems: state of the art. Luminescence. 2010; 25(6):409–418. https://doi.org/10.1002/bio.1203 PMID: 20354969

53. Poplová M, Sovka P, Cifra M. Poisson pre-processing of nonstationary photonic signals: Signals with equality between mean and variance. PLOS ONE. 2017; 12(12):e0188622. https://doi.org/10.1371/journal.pone.0188622 PMID: 29216207

54. Scholkmann F, Cifra M, Moraes TA, de Mello Gallep C. Using multifractal analysis of ultra-weak photon emission from germinating wheat seedlings to differentiate between two grades of intoxication with potassium dichromate. Journal of Physics: Conference Series. 2011; 329:012020.

55. Dlask M, Kukal J, Tran QV. Revisited Zero-Crossing Method for Hurst Exponent Estimation in Time Series. In: Martincik D, editor. Mathematical Methods in Economics Proceedings 2015. vol. 1. University of West Bohemia, Cheb, Czech Republic: University of West Bohemia, Plzen; 2015. p. 115–120.

56. Ondrušová B. Measurement Optimization and Analysis of Selected Physical and Chemical Effects on the Ultra-Weak Proton Emission from a Human Hand. CZECH TECHNICAL UNIVERSITY IN PRAGUE, Faculty of Electrical Engineering, Department of Circuit Theory; 2016. Available from: https://dspace.cvut.cz/handle/10467/64862?show=full.

57. Seber G, Wild C. Nonlinear regression. Hoboken, N.J.: Wiley; 2003.

58. Casella G, Berger RL. Statistical Inference. Cengage Learning; 2001. Available from: https://www.amazon.com/Statistical-Inference-George-Casella/dp/0534243126?SubscriptionId=0JYN1NVW651KCA56C102&tag=techkie-20&linkCode=xm2&camp=2025&creative=165953&creativeASIN=0534243126.

59. Anscombe FJ. The Transformation of Poisson, Binomial and Negative-Binomial Data. Biometrika. 1948; 35(3/4):246. https://doi.org/10.1093/biomet/35.3-4.246

60. Kristoufek L. Spectrum-based estimators of the bivariate Hurst exponent. PHYSICAL REVIEW E. 2014; 90(6).

61. Li C. Rescaled-range and power spectrum analyses on well-logging data. GEOPHYSICAL JOURNAL INTERNATIONAL. 2003; 153(1):201–212. https://doi.org/10.1046/j.1365-246X.2003.01893.x

62. Dietrich CR, Newsam GN. Fast and Exact Simulation of Stationary Gaussian Processes through Circulant Embedding of the Covariance Matrix. SIAM J Sci Comput. 1997; 18(4):1088–1107. https://doi.org/10.1137/S1064827592240555

63. Delignières D. Correlation Properties of (Discrete) Fractional Gaussian Noise and Fractional Brownian Motion. Mathematical Problems in Engineering. 2015; 2015:1–7.

64. Weiss M, Elsner M, Kartberg F, Nilsson T. Anomalous Subdiffusion Is a Measure for Cytoplasmic Crowding in Living Cells. Biophysical Journal. 2004; 87(5):3518–3524. https://doi.org/10.1529/biophysj.104.044263 PMID: 15339818

65. Aon MA, Cortassa S. On the fractal nature of cytoplasm. FEBS letters. 1994; 344(1):1–4. https://doi.org/10.1016/0014-5793(94)00321-1 PMID: 8181555

66. Ratto TV, Longo ML. Anomalous Subdiffusion in Heterogeneous Lipid Bilayers†. Langmuir. 2003; 19 (5):1788–1793. https://doi.org/10.1021/la0261803

67. Prasad J, Kopelman R. Fractal-like molecular reaction kinetics: solute photochemistry in porous membranes. Journal of Physical Chemistry. 1987; 91(2):265–266. https://doi.org/10.1021/j100286a007

68. Kopelman R. Fractal reaction kinetics. Science. 1988; 241(4873):1620–1626. https://doi.org/10.1126/science.241.4873.1620 PMID: 17820893

69. Bénichou O, Chevalier C, Klafter J, Meyer B, Voituriez R. Geometry-controlled kinetics. Nature Chemistry. 2010; 2(6):472–477. https://doi.org/10.1038/nchem.622 PMID: 20489716

70. Aon M. CHAOTIC DYNAMICS AND FRACTAL SPACE IN BIOCHEMISTRY: SIMPLICITY UNDERLIES COMPLEXITY. Cell Biology International. 2000; 24(8):581–587. https://doi.org/10.1006/cbir.2000.0572 PMID: 10924231

71. Saxton MJ. Wanted: A Positive Control for Anomalous Subdiffusion. Biophysical Journal. 2012; 103 (12):2411–2422. https://doi.org/10.1016/j.bpj.2012.10.038 PMID: 23260043

72. Martin DS, Forstner MB, Käs JA. Apparent Subdiffusion Inherent to Single Particle Tracking. Biophysical Journal. 2002; 83(4):2109–2117. https://doi.org/10.1016/S0006-3495(02)73971-4 PMID: 12324428

73. Oliver CJ, Pike ER. Measurement of low light flux by photon counting. Journal of Physics D: Applied Physics. 1968; 1(11):1459–1468. https://doi.org/10.1088/0022-3727/1/11/310

74. Foord R, Jones R, Oliver CJ, Pike ER. The Use of Photomultiplier Tubes for Photon Counting. Applied Optics. 1969; 8(10):1975. https://doi.org/10.1364/AO.8.001975 PMID: 20072559

75. Johnson FA, Jones R, McLean TP, Pike ER. Dead-Time Corrections to Photon Counting Distributions. Physical Review Letters. 1966; 16(13):589–592. https://doi.org/10.1103/PhysRevLett.16.589